# REPORT DOCUMENTATION PAGE

| 1. REPORT DATE (DD-MM-YYYY) | 2. REPORT TYPE | 3. DATES COVERED (From - To) |
|---|---|---|
| 14-02-2012 | Conference Proceedings | |

**4. TITLE AND SUBTITLE**
Estimating Errors in Satellite Retrievals of Bio-Optical Properties Due to Incorrect Aerosol Model Selection

**5a. CONTRACT NUMBER**

**5b. GRANT NUMBER**

**5c. PROGRAM ELEMENT NUMBER**
0602435N

**6. AUTHOR(S)**
Sean McCarthy, Richard Gould, James Richman, Courtney Kearney, Timothy Lawson

**5d. PROJECT NUMBER**

**5e. TASK NUMBER**

**5f. WORK UNIT NUMBER**
73-6467-01-5

**7. PERFORMING ORGANIZATION NAME(S) AND ADDRESS(ES)**
Naval Research Laboratory
Oceanography Division
Stennis Space Center, MS 39529-5004

**8. PERFORMING ORGANIZATION REPORT NUMBER**
NRL/PP/7330-11-0811

**9. SPONSORING/MONITORING AGENCY NAME(S) AND ADDRESS(ES)**
Office of Naval Research
One Liberty Center
875 North Randolph Street, Suite 1425
Arlington, VA 22203-1995

**10. SPONSOR/MONITOR'S ACRONYM(S)**
ONR

**11. SPONSOR/MONITOR'S REPORT NUMBER(S)**

**12. DISTRIBUTION/AVAILABILITY STATEMENT**
Approved for public release, distribution is unlimited.

20120217345

**13. SUPPLEMENTARY NOTES**

**14. ABSTRACT**
We examine the impact of incorrect atmospheric correction, specifically incorrect aerosol model selection, on retrieval of bio-optical properties from satellite ocean color imagery. Uncertainties in retrievals of bio-optical properties (such as chlorophyll, absorption and backscattering coefficients) from satellite ocean color imagery are related to a variety of factors, including errors associated with sensor calibration, atmospheric correction, and the bio-optical inversion algorithms. In many cases, selection of an inappropriate or erroneous aerosol model during atmospheric correction can dominate the errors in the satellite estimation of the normalized water-leaving radiances ($_nL_w$), especially over turbid, coastal waters. These errors affect the downstream bio-optical properties. Here, we focus on only the impact of incorrect aerosol model selection on the $_nL_w$ radiance estimates, through comparisons between Moderate- Resolution Imaging Spectroradiometer (MODIS) satellite data and in situ measurements from AERONET-OC (Aerosol Robotic NETwork - Ocean Color) sampling platforms.

**15. SUBJECT TERMS**
aerosol models, normalized water-leaving radiance, MODIS, AERONET-OC, atmospheric correction, ensembles

| 16. SECURITY CLASSIFICATION OF: | | | 17. LIMITATION OF ABSTRACT | 18. NUMBER OF PAGES | 19a. NAME OF RESPONSIBLE PERSON |
|---|---|---|---|---|---|
| a. REPORT | b. ABSTRACT | c. THIS PAGE | UU | 10 | Richard Gould |
| Unclassified | Unclassified | Unclassified | | | 19b. TELEPHONE NUMBER (Include area code) 228-688-5587 |

# Estimating errors in satellite retrievals of bio-optical properties due to incorrect aerosol model selection

Sean C. McCarthy[a], Richard W. Gould, Jr.[b], James Richman[b], Courtney Kearney[c], Adam Lawson[b]

[a]NRC PostDoc; [b]Naval Research Laboratory, Stennis Space Center, MS, 39529; [c]ASEE PostDoc

## ABSTRACT

We examine the impact of incorrect atmospheric correction, specifically incorrect aerosol model selection, on retrieval of bio-optical properties from satellite ocean color imagery. Uncertainties in retrievals of bio-optical properties (such as chlorophyll, absorption and backscattering coefficients) from satellite ocean color imagery are related to a variety of factors, including errors associated with sensor calibration, atmospheric correction, and the bio-optical inversion algorithms. In many cases, selection of an inappropriate or erroneous aerosol model during atmospheric correction can dominate the errors in the satellite estimation of the normalized water-leaving radiances ($_nL_w$), especially over turbid, coastal waters. These errors affect the downstream bio-optical properties. Here, we focus on only the impact of incorrect aerosol model selection on the $_nL_w$ radiance estimates, through comparisons between Moderate-Resolution Imaging Spectroradiometer (MODIS) satellite data and in situ measurements from AERONET-OC (Aerosol Robotic NETwork – Ocean Color) sampling platforms.

**Keywords:** aerosol models, normalized water-leaving radiance, MODIS, AERONET-OC, atmospheric correction, ensembles

## 1. INTRODUCTION

The main challenge in atmospheric correction is the estimation and the removal of the path radiance from the top-of-atmosphere (TOA) radiance values recorded by the satellite sensor [1]. The path radiance contains both Rayleigh and aerosol scattering components and can contribute about 90% of the TOA radiance [2,3]. In the current version of the NASA ocean color atmospheric correction processing code, there are 80 aerosol models to choose from to calculate spectral aerosol radiance [4]. This is a more complex modeling system than Gordon and Wang's previous 12 model set [5]. Based on the spectral slope of the aerosol reflectance in the NIR bands, the two most appropriate aerosol models (from the entire set of 80 models) are retrieved and used for estimation of the aerosol radiance in the visible wavelengths. Are we appropriately selecting these models?

We have tested all 80 aerosol models individually with data sets collected from three AERONET-OC sites (Venice, Martha's Vineyard, and Gulf of Mexico) [6,7,8]. First, we derive $_nL_w$ from MODIS 1km resolution imagery at the locations of the AERONET-OC sites, using the aerosol models selected automatically from the standard atmospheric correction scheme [9]. We compare these satellite values to the in situ measurements. We then reprocess the satellite imagery using all 80 aerosol models individually and again compare the products to the in situ measurements. This is performed in order to determine the "optimal" aerosol model for each individual point at the AERONET-OC location for each individual scene (MODIS image). The optimal model is the aerosol model that yields $_nL_w$ closest to the in situ values. We determine the optimal aerosol model at a single wavelength and can either use that model for the remaining visible wavelengths or determine new optimal aerosol models at each remaining visible wavelength.

Section 2 (Atmospheric Correction Using Aerosol Models) briefly describes how aerosol models are used during atmospheric correction. This section also describes the set of aerosol models used, how those models are chosen during atmospheric correction, and possible errors associated with the models. Section 3 (Automatic vs Optimal Model Selection) compares the result of standard, automatic selection of aerosol models to the optimal model selection. This section shows that out of the possible 80 aerosol models to choose, there is most likely a set of models that will produce $_nL_w$ values that closely match the in situ values. However, during standard atmospheric correction, we are usually not properly selecting these models. This paper concludes with Section 4 (Conclusions) and Section 5 (Future Work).

## 2. ATMOSPHERIC CORRECTION USING AEROSOL MODELS

The top of the atmosphere (TOA) radiance is defined as follows:

$L_t(\lambda) = L_r(\lambda) + L_a(\lambda) + L_{ra}(\lambda) + t(\lambda) L_{wc}(\lambda) + T(\lambda) L_g(\lambda) + t(\lambda) t_0(\lambda) \cos\theta_0 [L_w(\lambda)]_N$, where $\lambda$ is wavelength, $L_t(\lambda)$ is top-of-atmosphere radiance, $L_r(\lambda)$ is the radiance due to scattering by the air molecules (Rayleigh scattering) [10,11,12], $L_a(\lambda)$ is the radiance due to scattering by aerosols, $L_{ra}(\lambda)$ is the multiple interaction term between molecules and aerosols, $t(\lambda)$ is the diffuse transmittance of the atmosphere from the surface to the sensor, $L_{wc}(\lambda)$ is the radiance due to whitecaps on the sea surface [13,14], $T(\lambda)$ is the direct transmittance from the surface to the sensor, $L_g(\lambda)$ is the specular reflection of direct sunlight off the sea surface (sun-glitter) [15], $t_0(\lambda)$ is the diffuse transmittance of the atmosphere from the sun to the surface, $\theta_0$ is the solar-zenith angle, and $[L_w(\lambda)]_N$ is the normalized water-leaving radiance ($_nL_w$) due to photons that penetrate the sea surface and are backscattered out of the water [16].

The goal of atmospheric correction is to retrieve $_nL_w$ accurately. The main challenge in atmospheric correction is the removal of $L_{path}(\lambda)$ from $L_t(\lambda)$, where $L_{path}(\lambda) = L_r(\lambda) + L_a(\lambda) + L_{ra}(\lambda)$. $L_{path}(\lambda)$ contributes about 90% of the TOA radiance. $L_r(\lambda)$ can be removed from $L_{path}(\lambda)$ by using standard radiative transfer methods. The remaining part of $L_{path}(\lambda)$, $L_a(\lambda) + L_{ra}(\lambda)$, is estimated from $L_t(\lambda)$ in the NIR wavelengths. We assume that $_nL_w$ is 0 in clear, open-ocean regions in the NIR wavelengths. However, this is not true in turbid, coastal areas. By assuming that $_nL_w$ is 0 in the NIR, this provides $L_a(\lambda) + L_{ra}(\lambda)$. Based on $L_a(\lambda) + L_{ra}(\lambda)$ in the NIR, an estimate is made of $L_a(\lambda) + L_{ra}(\lambda)$ in the visible. There have been studies conducted over the past decade of the optical properties of aerosol types [17,18,19,20,21,22,23]. This has lead to using aerosol modeling to extrapolate from the NIR to the visible bands. Figure 1 shows these components over multiple wavelengths for Gulf of Mexico, May 4, 2010.
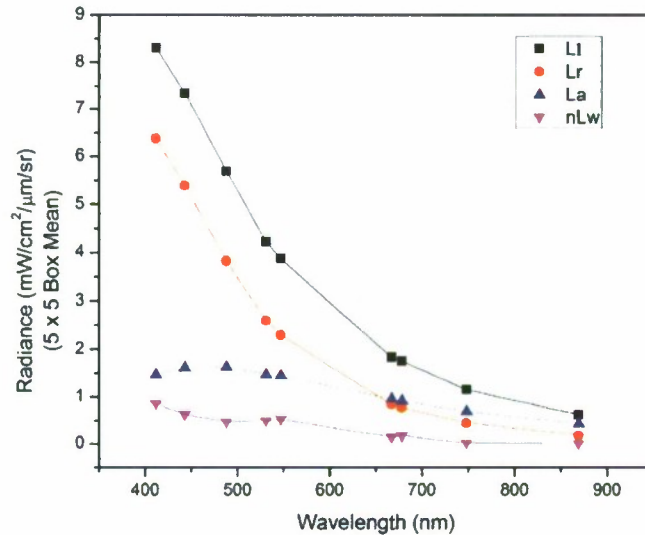


Figure 1. MODIS-retrieved $L_t$, $L_r$, $L_a$, and $_nL_w$ for 412, 443, 488, 531, 547, 667, 748, and 869 (nm) wavelengths at the AERONET-OC location for Gulf of Mexico, May 4, 2010

There are 80 aerosol models (indexed 0 to 79) to choose from to compute $L_a + L_{ra}$ during atmospheric correction. These aerosol models are used for computing $L_a(\lambda) + L_{ra}(\lambda)$. The most significant digit in the aerosol model number (ex: the 6 in model 64) denotes relative humidity index. The least significant digit denotes a particle size fraction index. Table 1 lists the different relative humidity and size fraction percentages, along with their corresponding aerosol model index. Regarding the size fractions, a size fraction of 20% denotes 20% fine mode and 80% coarse mode. For example, model 64 corresponds to a relative humidity of 90% and a size fraction of 20%, with 20% being fine mode and 80% being coarse mode.

Table 1. Relative humidity and size fraction percentages and corresponding model index, models ranging from 0 to 79

| Relative Humidity Index (Most Significant Digit in Model Index) | Relative Humidity Percentage | Size Fraction Index (Least Significant Digit in Model Index) | Size Fraction Percentage |
|---|---|---|---|
| 0 | 30% | 0 | 95% |
| 1 | 50% | 1 | 80% |
| 2 | 70% | 2 | 50% |
| 3 | 75% | 3 | 30% |
| 4 | 80% | 4 | 20% |
| 5 | 85% | 5 | 10% |
| 6 | 90% | 6 | 5% |
| 7 | 95% | 7 | 2% |
| | | 8 | 1% |
| | | 9 | 0% |

During standard atmospheric processing, there are two aerosol models chosen to bound $L_a(\lambda) + L_{ra}(\lambda)$ in the NIR. The aerosol models are chosen by determining which two aerosol models bound $\epsilon(748,869)$ the tightest, where $\epsilon(748,869)$ is a ratio for wavelengths 748/869 [24]. This ratio is used to select bounding aerosol models. The relative humidity index is calculated before $\epsilon(748,869)$ is calculated, so $\epsilon(748,869)$ is used to select the size fraction index. Once the two bounding aerosol models are chosen based on $\epsilon(748,869)$, interpolation is performed between the two models and then $L_a(\lambda) + L_{ra}(\lambda)$ is retrieved from the aerosol model lookup tables.

To examine the effect of $\epsilon(748,869)$ and model selection on retrieved $_nL_w$, we tested all 80 aerosol models individually for a single clear day, January 9, 2009, in Venice. Instead of using two bounding aerosol models, we used a fixed aerosol model to study the effects of all 80 aerosol models on retrieved $_nL_w$. The results are displayed in Figure 2.
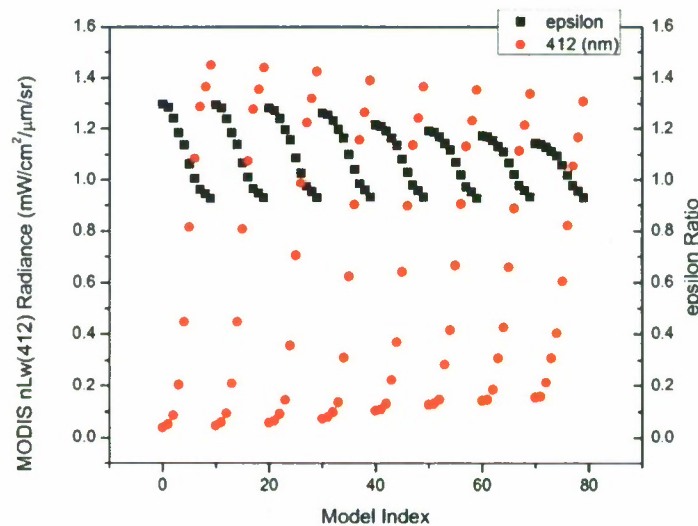


Figure 2. MODIS retrieved epsilon and $_nL_w(412)$ for all 80 aerosol models at the AERONET-OC location for Venice, Jan 9, 2009

Figure 2 shows that relative humidity has a low impact on retrieved $_nL_w$ values. To describe the impact on relative humidity and size fraction on retrieved $_nL_w$ values, consider an example using the values in Figure 2 where the bounding aerosol models selected are 14 (relative humidity of 50%, size fraction of 20%) and 15 (relative humidity of 50%, fine-mode fraction of 10%). Model 14 and 15 depict $_nL_w(412) \approx 0.45$ and $_nL_w(412) \approx 0.81$, respectively. There is significant interpolation between these two models to derive the actual $_nL_w(412)$ value. This is due to the distance in $_nL_w(412)$ values because of the size fraction, not the relative humidity. If the model selection is off by 1 or 2 model

indices with regard to the size fraction, then there are large errors associated with the retrieval of $_nL_w(412)$. Even if the models are correctly selected, the interpolation between the two models can still lead to large errors in $_nL_w(412)$. However, the relative humidity can be incorrectly selected, and as long as the size fraction is correct, the retrieved $_nL_w(412)$ value should still match closely to the in situ value.

To further demonstrate how size fraction is a larger factor than relative humidity in retrieved $_nL_w$ values, suppose we now have bounding aerosol models 74 and 75 from Figure 2 instead of models 14 and 15 (relative humidity changes from 50% to 95% and size fraction stays the same). For models 74 and 75, $_nL_w(412) \approx 0.4$ and $nLw(412) \approx 0.6$, respectively. In the example in the preceding paragraph, bounding models 14 and 15 produce $_nL_w(412) \approx 0.63$ (halfway between models 14 and 15). Halfway between models 74 and 75, $_nL_w(412) \approx 0.5$. The relative humidity could be off by several model indices (in this case 6 models, in regards to the relative humidity index), and the $_nL_w(412)$ error $\approx 0.13$. To illustrate the impact of the size fraction, now suppose the bounding aerosol models are 15 and 16 instead of 14 and 15. For models 15 and 16, $_nL_w(412) \approx 0.81$ and $_nL_w(412) \approx 1.09$, respectively. $_nL_w(412)$ interpolated midway between these two models produces $_nL_w(412) \approx 0.95$. That is a difference of 0.32 from models 14 and 15. This shows that if incorrect aerosol models are chosen in relation to the size fraction, there can be significant errors in the retrieved $_nL_w$ values, but smaller errors will result from incorrect model selection based on relative humidity.

## 3. AUTOMATIC VS OPTIMAL AEROSOL MODEL SELECTION

Using the aerosol models selected automatically from the SeaWiFS/MODIS atmospheric correction algorithm [25], we derive $_nL_w$ from MODIS 1km resolution imagery at the locations of the AERONET-OC sites (Martha's Vineyard, Venice, and Gulf of Mexico). We compare these satellite values to the AERONET-OC measurements (matchups within 3 hours, at least 50% valid pixels in a 5 x 5 box centered around the in situ pixel). We then reprocess the satellite imagery using all 80 aerosol models. Rather than standard processing automatically selecting two bounding aerosol models, a single aerosol model is used when determining the optimal model. The processing is repeated 80 different times, once for each model. After reprocessing with all 80 individual aerosol models, we again compare the derived $_nL_w$ products to the in situ measurements. The model yielding the closest $_nL_w$ value to the in AERONET-OC value is selected as the "optimal" model. For each scene in the data set, we are only interested in the 5 x 5 box centered around the in situ pixel.

For the analysis of Martha's Vineyard, 2010, we determine the optimal aerosol model for $_nL_w$ at the AERONET-OC location at selected visible wavelengths. Figure 3 displays the $_nL_w$ matchups for satellite standard processing vs in situ, as well as satellite processing with optimal aerosol model selection vs in situ. The errors (calculated as the absolute value of ((MODIS – AERONET-OC) / AERONET-OC)*100) are greatly reduced with the optimal model selection.
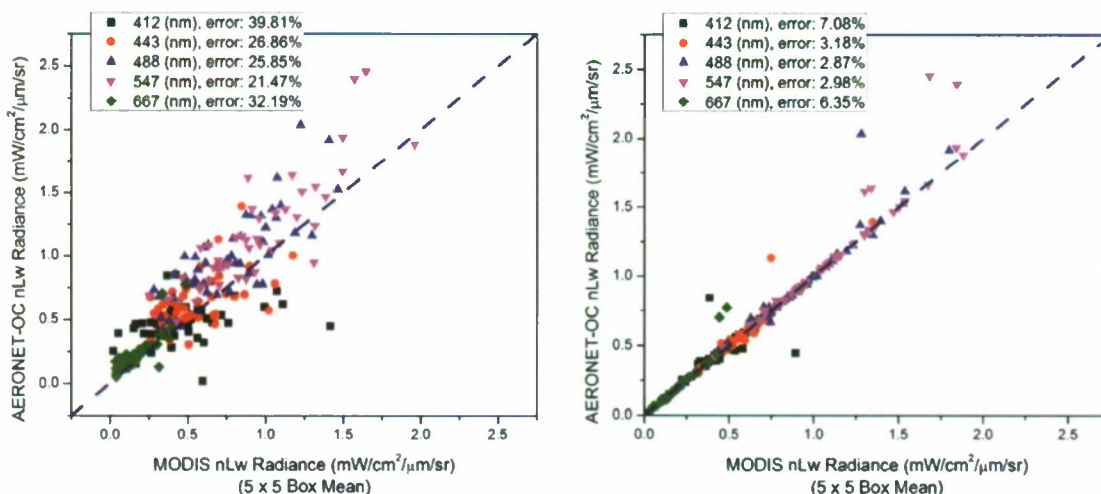


Figure 3. Automatic aerosol model selection (left image) vs optimal aerosol model selection (right image) used to produce $_nL_w$ at 412, 443, 488, 547, and 667 wavelengths for Martha's Vineyard, 2010

Using the same data set seen in Figure 3, in Figure 4 we show the optimal aerosol model selected for computing $_nL_w(412)$, as well as the bounding aerosol models selected during standard atmospheric processing. Figure 4 shows a wide spread of optimal aerosol model selections throughout 2010 for Martha's Vineyard. This is due to relative humidity index varying throughout the optimal models chosen for this data set. The optimal model for a particular sample in the data set is based on how close $_nL_w$ is to the AERONET-OC value. Because of this, relative humidity is not really used since size fraction plays a more important role in retrieved $_nL_w$ values. This does not mean that the optimal model is stating that the relative humidity is incorrect during standard atmospheric correction. It also does not mean that there are not other models that are capable of producing values that closely match the AERONET-OC values. For example, in Fig. 2 we can see that models 36, 46, 56, and 66 all yield similar $_nL_w$ values ($\sim 0.9$).

During standard atmospheric correction, the modmin bounding aerosol model's index is supposed to be one higher than the modmax bounding aerosol model. This is not always the case. There are four points in Figure 4 where modmin and modmax are the same. They are the 5 x 5 box means centered around the AERONET-OC station for days 80, 162, 231, and 240. This is the case when $\epsilon(748,869)$ does not fall between the lookup tables for two bounding aerosol models. When modmin and modmax are the same, it means that $\epsilon(748,869)$ is either lower than the $\epsilon(748,869)$ in the lookup tables for the lowest available bounding aerosol model or higher than the $\epsilon(748,869)$ in the lookup tables for the highest available bounding aerosol model. When this occurs, it almost always leads to a poor estimate of the aerosol composition, which in turn results in an erroneous estimate of $_nL_w$ values.
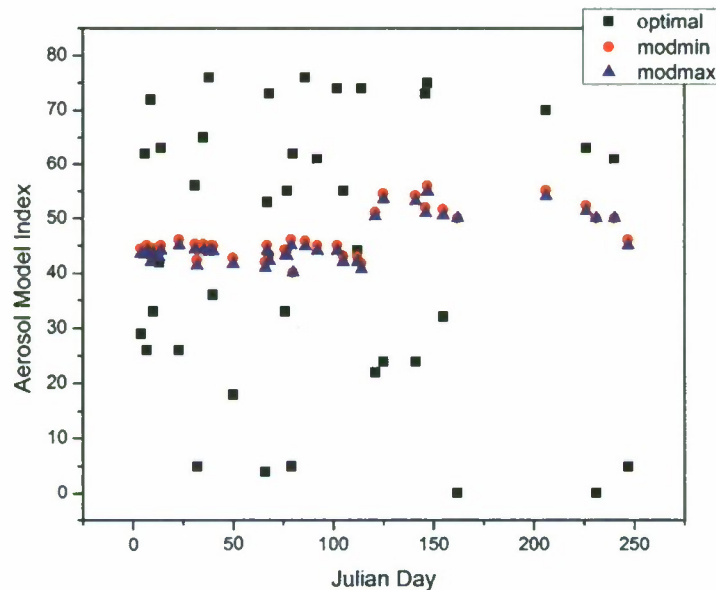


Figure 4. Automatic aerosol selection vs optimal aerosol model selection for $_nL_w(412)$ for Martha's Vineyard, 2010

Figure 5 uses the same data set used in Figures 3 and 4. In Figure 5, we demonstrate how well automatic aerosol selection (modmin and modmax bounding aerosol models) produces $_nL_w(412)$ values when the size fraction matches the size fraction of the optimal aerosol model. We also show results for when the size fraction for the bounding aerosol models do not match the optimal model. The $_nL_w(412)$ values are matched against AERONET-OC $_nL_w(412)$ values. For each data point, we are comparing how well the size fraction (we are only looking at size fraction here and not relative humidity) is automatically selected compared to the optimal size fraction for each data point in Figure 4. Because the automatic aerosol selection uses two bounding aerosol models, and we only found a single optimal aerosol model for each data point, we must determine how close the optimal size fraction is to the size fractions computed for the bounding aerosol models during the automatic aerosol selection process of standard atmospheric correction. In Figure 5, all of the data points used for Martha's Vineyard 2010 are separated into four groups. The first group (modmax <= optimal <= modmin) is for any data points where the optimal size fraction is in between the bounding aerosol models. This means that the size fraction is likely to have been correctly selected during standard atmospheric

correction. For example, day 9 has an optimal size fraction of 2, a 5 x 5 box average for modmin of 2.96, and a 5 x 5 box average for modmax of 1.96. To clarify, individual points in the scene do not have a fractional aerosol model index. For modmax to have a value of 1.96, 24 of 25 points in the 5 x 5 box have a value of 2, and 1 of 25 points in the 5 x 5 box have a value of 1. The second group (modmax - 1 <= optimal <= modmin + 1) is for data points where the size fractions for the bounding aerosol models do not fit in the first group, but are only plus or minus 1 size fraction away from the optimal size fraction. For example, day 10 has an optimal size fraction of 3, a 5 x 5 box average for modmin of 4.44, and a 5 x 5 box average for modmax of 3.44. Day 10 belongs in the second group because (3.44 – 1 <= 3 <= 4.44 + 1). The third group (modmax - 2 <= optimal <= modmin + 2) contains points +- 3 size fraction indices, excluding those in groups one and two. The fourth group (modmax - 3+ <= optimal <= modmin + 3+) is for all data points that do not fit in groups one, two, or three.

For Figure 5, we remove the data points in the first group where the bounding aerosol models have the same size fraction (modmin and modmax are both equal to zero). These are treated as bad data points, for reasons previously discussed. There are 11 data points in the first group, 12 in the second group, 6 in the third group, and 7 in the fourth group. This means that standard processing accurately selected bounding aerosol models for only 11 of the total 36 points. The average error for the data points in the first group is 19.26%, 37.85% for the second group, 35.60% for the third group, and 50.4% for the fourth group. This shows that if the bounding aerosol models' fine fraction is chosen correctly, the $_nL_w$ estimates ($_nL_w(412)$ in this case) are reasonably accurate. If the size fraction is off by just one, in either direction, it can greatly impact retrieved $_nL_w$ values.
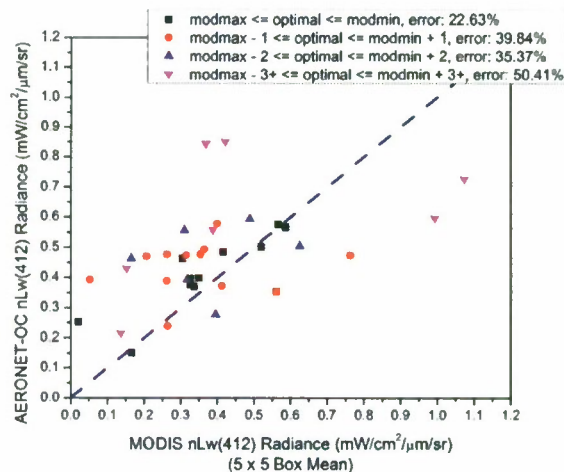


Figure 5. Size fraction sensitivity analysis for automatic aerosol selection (size fraction) vs AERONET-OC for $_nL_w(412)$ for Martha's Vineyard, 2010

To examine model variability, in Figure 6 we show the ensemble of retrived $_nL_w$ values from all 80 models from the MODIS image on 25 July 2010 at the Martha's Vineyard AERONET-OC site, compared to the in situ measurement. During standard automated processing, the 5 x 5 box mean surrounding the AERONET-OC site is 1.07344, and the two bounding aerosol models are 54 and 55. The optimal model is model 70, which produces an $_nL_w(412)$ of 0.7298, which is almost identical to the in situ value of 0.7254. Standard processing shows a relative humidity of 85% (since the model index is in the 50s), and the optimal model shows a relative humidity of 95% (since the model index is in the 70s). The significant difference in the bounding models selected during standard processing and the optimal model is the size fraction. The modmax bounding model (model 54) produces a value of 0.9222. The modmin bounding model (model 55) produces a value of 1.1973. We can take the mean between these two models to produce the standard processing $_nL_w(412)$ value of 1.07344. Despite the optimal aerosol model being 70 in this example, there are multiple aerosol models that can select an $_nL_w$ value that matches closely to the AERONET-OC's measurement. If we stay in the standard processing relative humidity (85%), models 52 and 53 could be used to produce a better $_nL_w$ value. In this example, $\epsilon(748,869)$ is computed and incorrect bounding aerosol models are chosen. Rather than models 54 and 55 being chosen during standard atmospheric correction, if models 52 and 53 were chosen, the $_nL_w$ value would match closely to the

in situ value. This is an example of how during standard atmospheric correction, whenever MODIS values are 10% off or more than the AERONET-OC values, it is usually because the bounding aerosol models were incorrectly selected.
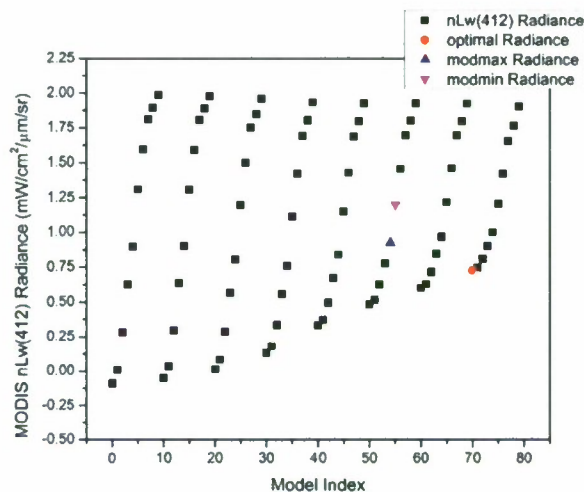


Figure 6. MODIS retrieved $_nL_w(412)$ for all 80 aerosol models at the AERONET-OC location for Martha's Vineyard, July 25, 2010

For the analysis of Venice, 2010, we determine the optimal aerosol model at $_nL_w(412)$ for 53 individual points (each point is a separate MODIS satellite image; each individual image represents a single day) at the AERONET-OC location. We then use that optimal model for the remaining wavelengths, instead of calculating the optimal model for each wavelength as we did with the Martha's Vineyard evaluation. Figure 7 is a composite figure of the $_nL_w$ results. The images in Figure 7 show that using the optimal model for nLw(412) has good performance in the remaining visible wavelengths.
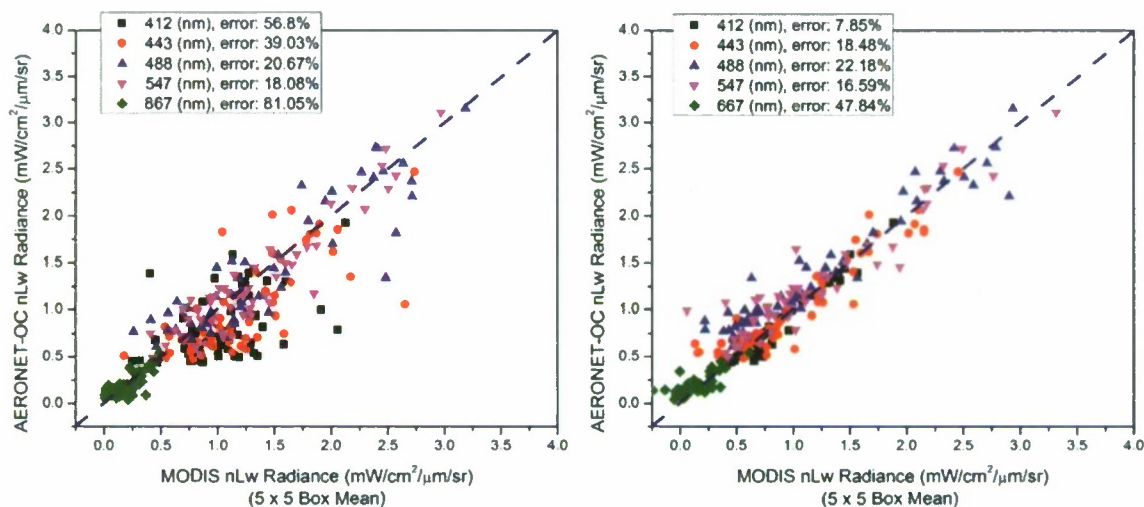


Figure 7. Automatic aerosol model selection (left image) vs optimal aerosol model selection (right image) used to produce $_nL_w$ at 412, 443, 488, 547, and 667 wavelengths for Venice, 2010

Figure 8 shows the results from a similar analysis for the Gulf of Mexico AERONET-OC site. However, the Gulf of Mexico does not have as many valid points for 2010 as Martha's Vineyard or Venice. This is due to a large amount of cloud coverage during the year, as well as the AERONET-OC station being unavailable for a few months of the year due to instrument calibration. One area of interest in this analysis is that for two of the MODIS images, there are no good aerosol models available that are capable of producing a matchup close to the corresponding in situ value. There are five data points in Figure 8 that correspond to these two MODIS images (two $_nL_w(412)$ values, two $_nL_w(443)$ values, and one $_nL_w(547)$ value). Three of these five values (one $_nL_w(412)$ value, one $_nL_w(443)$ value, and one $_nL_w(488)$ value) correspond to day 176. For day 176, both modmin and modmax are equal to forty, meaning these bounding aerosol models selected during standard atmospheric correction are incorrectly chosen. In this case, there is no possible aerosol model that can be used to produce a good result for $_nL_w(412)$ for day 176. This is an instance where the MODIS image has sporadic cloud coverage, as well as haze. During processing, not enough pixels were flagged, thus considering this day to be a valid day. When there are no possible aerosol models capable of producing values that closely match AERONET-OC values, it is likely because pixels were not flagged as invalid pixels when they should be.
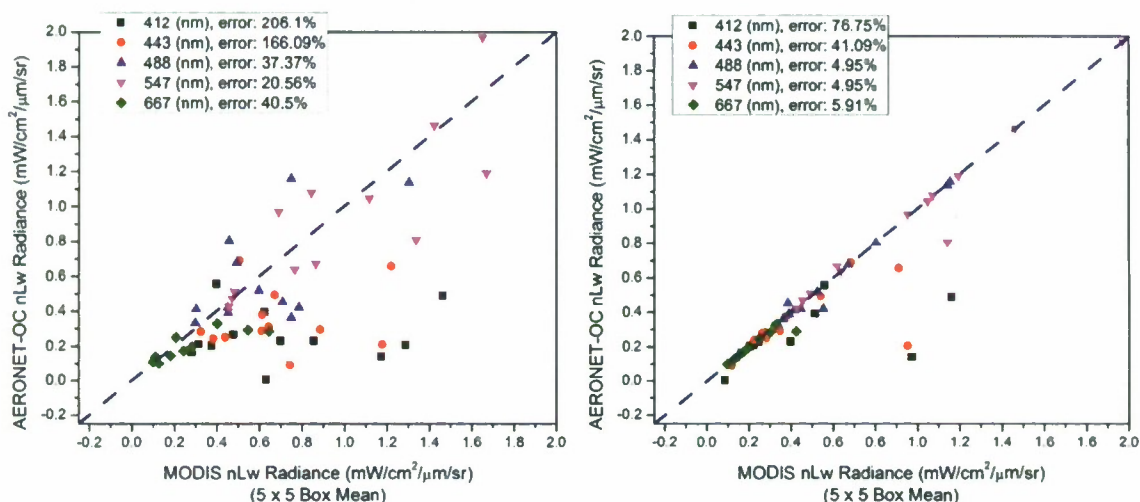


Figure 8. Automatic aerosol model selection (left image) vs optimal aerosol model selection (right image) used to produce $_nL_w$ at 412, 443, 488, 547, and 667 wavelengths for Gulf of Mexico, 2010

## 4. CONCLUSIONS

In this paper, we have compared satellite $_nL_w$ retrievals to in situ for Martha's Vineyard, Venice, and the Gulf of Mexico. During standard automated atmospheric correction, selection of inappropriate or erroneous bounding aerosol models can dominate the errors in the satellite estimation of $_nL_w$. Errors in $_nL_w$ will in turn affect downstream bio-optical properties. When bounding aerosol models are incorrectly chosen during atmospheric correction, it is the size fraction, rather than the relative humidity, that has the most impact on retrieved $_nL_w$ values. If bounding aerosol models are incorrectly selected, there is usually another set of bounding aerosol models within the same relative humidity index that are capable of correctly estimating aerosol values.

## 5. FUTURE WORK

There usually exists a temporal or regional trend of over-estimation or under-estimation of $_nL_w$ satellite values. Where a trend exists, we can devise a method for developing ensembles based on a sampling of bounding aerosol models. These ensembles will be used in creating new $_nL_w$ values that better resemble values from nearby AERONET-OC stations.

We also need to expand our study from a concentrated 5 x 5 box mean around the AERONET-OC point to the entire scene. If we change the bounding aerosol models used during atmospheric correction, we would like to determine

if the change in bounding aerosol models can be used across the entire scene. This can be evaluated by comparing chlorophyll examinations at the AERONET-OC site to other chlorophyll samples taken somewhere else in the scene, perhaps during a cruise. We need to further examine wavelengths other than 412 since the chlorophyll algorithms use other visible wavelengths.

Another method for improving $_nL_w$ estimates is to expand the set of aerosol models. More models are needed in the middle of the size fraction range to reduce interpolation between bounding aerosol models.

## ACKNOWLEDGEMENTS

## REFERENCES

[1] Wang, M. and Gordon, H. R., "A simple, moderately accurate, atmospheric correction algorithm for SeaWiFS," Remote Sens. Environ. 50: 231-239 (1994).

[2] Antoine, D. and Morel, A., "A multiple scattering algorithm for atmospheric correction of remotely sensed ocean color (MERIS instrument): principle and implementation for atmospheres carrying various aerosols including absorbing ones," Int. J. Remote Sens. 20: 1875-1916 (1999).

[3] Antoine, D. and Morel, A., "Relative importance of multiple scattering by air molecules and aerosols in forming the atmospheric path radiance in the visible and near-infrared parts of the spectrum," Appl. Opt. 37: 2245-2259 (1998).

[4] Ahmad, Z., Franz, B. A., McClain, C. R., Kwiatkowska, E. J., Werdell, J., Shettle, E. P. and Holben, B.N., "New aerosol models for the retrieval of aerosol optical thickness and normalized water-leaving radiances from the SeaWiFS and MODIS sensors over coastal regions and open oceans." Appl. Opt., Vol. 49, No. 29, 5545-5558 (2010).

[5] Gordon, H. R. and Wang, M., "Retrieval of water-leaving radiance and aerosol optical thickness over the oceans with SeaWiFS: a preliminary algorithm," Applied Optics, Vol. 33, No. 3, 443-452 (1994).

[6] http://aeronet.gsfc.nasa.gov/new_web/photo_db/MVCO.html

[7] http://aeronet.gsfc.nasa.gov/new_web/photo_db/Venise.html

[8] http://aeronet.gsfc.nasa.gov/new_web/photo_db/WaveCIS_Site_CSI_6.html

[9] Salomonson, V. V., Barnes, W. L, Maymon, P. W., Montgomery, H. E. and Ostrow, H., "MODIS: advanced facility instrument for studies of the earth as a system," IEEE Trans. Geosci. Remote Sensing 27, 145-152 (1989).

[10] Gordon, H. R., Brown, J. W. and Evans, R. H., "Exact Rayleigh scattering calculations for use with the Nimbus-7 Coastal Zone Color Scanner," Appl. Opt. 27: 862-871 (1988).

[11] Wang, M., "A refinement for the Rayleigh radiance computation with variation of the atmospheric pressure," Int. J. Remote Sens. 26: 5651-5663 (2005).

[12] Wang, M., "The Rayleigh lookup tables for the SeaWiFS data processing: Accounting for the effects of ocean surface roughness," Int. J. Remote Sens. 23: 2693-2702 (2002).

[13] Frouin, R., Schwindling, M., Deschamps, P. Y., "Spectral reflectance of sea foam in the visible and near infrared: In situ measurements and remote sensing implications," J. Geophys. Res. 101(C6): 14,361-14,372 (1996).

[14] Gordon, H. R. and Wang, M., "Influence of oceanic whitecaps on atmospheric correction of ocean-color sensor," Appl. Opt. 33: 7754-7763 (1994).

[15] Wang, M. and Bailey, S., "Correction of the sun glint contamination on the SeaWiFS ocean and atmosphere products," Appl. Opt. 40: 4790-4798 (2001).

[16] Gordon, H. R. and Wang, M., "Surface roughness considerations for atmospheric correction of ocean color sensors. 2: Error in the retrieved water-leaving radiance," Appl. Opt. 31: 4261-4267 (1992).

[17] Dubovik, O. and King, M. D., "A flexible inversion algorithm for retrieval of aerosol optical properties from sun and sky radiance measurements," J. Geophys. Res. 105, 20673-20696 (2000).

[18] Dubovik, O., Holben, B., Eck, T. F., Smirnov, A., Kaufman, Y. J., King, M. D., Tanre, D. and Slutsker, I., "Variability of absorption and optical properties of key aerosol types observed in worldwide locations," J. Atmos. Sci. 59, 590-608 (2002).

[19] Dubovik, O., Smirnov, A., Holben, B., King, M. D., Kaufman, Y. J., Eck, T. F. and Slutsker, I., "Accuracy assessments of aerosol optical properties retrieved from AERONET sun and sky radiance measurements," J. Geophys. Res. 105, 9791-9806 (2000).

[20] Gordon, H. R., Du, T., Zhang, T., "Remote sensing of ocean color and aerosol properties: resolving the issue of aerosol absorption," Appl. Opt. 36: 8670-8684 (1997).

[21] Holben, B. N., Eck, T. F., Slutsker, I., Tanre, D., Buis, J. P., Setzer, A., Vermote, E., Reagan, J. A., Kaufman, Y., Nakajima, T., Lavenu, F., Jankowiak, I. and Smirnov, A., "AERONET - A federated instrument network and data archive for aerosol characterization," Remote Sens. Environ. 66, 1-16 (1998).

[22] O'Neill, N. T., Pietras, C., Pinker, R. T., Voss, K. and Zibordi, G., "Am emerging ground-based aerosol climatology: aerosol optical depth from AERONET," J. Geophys. Res. 106, 12067-12097 (2001).

[23] Sinyuk, A., Dubovik, O., Holben, B., Eck, T. F., Breon, F-M., Martonchik, J., Kahn, R., Diner, D. J., Vermote, E. F., Roger, J-C., Lapyonok, T. and Slutsker, I., "Simultaneous retrieval of aerosol and surface properties from a combination of AERONET and satellite," Remote Sens. Environ. 107, 90-108, doi:10.1016/j.rse.2006.07.022 (2007).

[24] Wang, M., "Extrapolation of the aerosol reflectance from the near-infrared to the visible: the single-scattering epsilon vs multiple-scattering epsilon method," Int. J. Remote Sens. 25: 3637-3650 (2004).

[25] Wang, M., "The SeaWiFS atmospheric correction algorithm updates," Report No. Vol. 9, NASA Tech. Memo. 2000-206892, Hooker, S. B., Firestone, E. R. (Eds.), NASA Goddard Space Flight Center, Greenbelt, Maryland (2000).